Materials Today Chemistry 22 (2021) 100549

Contents lists available at ScienceDirect

Materials Today Chemistry

journal homepage: www.journals.elsevier.com/materials-today-chemistry/

Effect of thermal annealing on a bilayer polyvinyl alcohol/polyacrylic acid electrospun hydrogel nanofibres loaded with doxorubicin and clarithromycin for a synergism effect against osteosarcoma cells

B.S. Chee [a], G.G. de Lima [a, b], T.A.M. de Lima [a], V. Seba [a], C. Lemarquis [a, c], B.L. Pereira [a, b], M. Bandeira [a], Z. Cao [a], M. Nugent [a, *]

[a] Materials Research Institute, Athlone Institute of Technology, Athlone, Ireland
[b] Federal University of Paraná, Programa de Pós-Graduação em Engenharia e Ciência dos Materiais – PIPE, Curitiba, Brazil
[c] Institut Universitaire de Technologie de Lannion, France

ARTICLE INFO

Article history:
Received 15 April 2021
Received in revised form
22 July 2021
Accepted 2 August 2021
Available online xxx

Keywords:
Hydrogels
Electrospinning
Nanofibres
Physical crosslinking
Drug delivery

ABSTRACT

Polyvinyl alcohol/polyacrylic acid (PVA/PAA) bilayer hydrogel nanofibres were successfully fabricated by electrospinning and physically crosslinked via heat treatment. The effects of the thermal annealing process on the structure, morphology, swelling, thermal properties and hydrophilicity of electrospun nanofibres were investigated. In addition, these membranes were also used to incorporate doxorubicin and clarithromycin for osteosarcoma treatment, one in each layer. These drugs were used because it is hypothesized in this work that a synergism occurs between both drugs. So, these membranes were analyzed towards their dual-drug release and potential cytotoxicity towards the U2OS human osteosarcoma cell line. Moreover, the water contact angle, disintegration, swelling and weight loss studies confirmed the rapid swelling and improved water stability of the annealed PVA/PAA bilayer nanofibres. The annealed bilayer nanofibres exhibited an increase in the average diameter and degree of crystallinity. In addition, the results revealed that a variation occurred in the degree of hydrophilicity of annealed PVA/PAA bilayer nanofibres. The PAA nanofibres surface exhibited higher hydrophilicity than the PVA nanofibres surface. Drug delivery presented to be as fast rate release for clarithromycin and slow-rate release for doxorubicin, which may be advantageous because both drugs exhibited to be synergetic for certain dosages presenting the combination of the drugs higher than 50% of cell inhibition, while these membranes had higher inhibition values (up to 90%), which was attributed to the PAA but also the drugs. These unique properties are of potential interest in drug delivery applications for dual drug delivery where the tunability of surfaces is desirable.

1. Introduction

Nanofibres are used in a wide range of biomedical and industrial applications, including wound healing [1], biosensors [2], water filtration [3] and food packaging [4]. Within the various techniques to produce continuous nanofibres, electrospinning stands out as a versatile technique. Our lab has used this technique in a number of applications such as brain implant [5], wound dressing [6], bone implant and drug delivery. A wide variety of aqueous polymer solutions such as polyvinyl alcohol (PVA), polyacrylic acid (PAA), poly (2-hydroxyethyl methacrylate) and poly(N-isopropyl acrylamide) can be used for electrospinning [7], which directly relates to the properties of the fiber and can be modified using crosslinking agents to confer specific characteristic and, in many cases, SMART configurations [8]. In this study, PVA and PAA were chosen to fabricate a bilayer electrospun nanofibre as they present a well-formed cross-linked hydrophilic polymer structure, which can retain large amounts of water and biological fluids [9]. Moreover, the PVA/PAA bilayer nanofibres exhibit the heterogeneous properties from both PVA (i.e. biocompatible, biodegradable, water-soluble and non-carcinogenic) and PAA (i.e. pH-sensitive) [10].

The strong interaction of inter-polymer hydrogen bonding between PVA and PAA results in a completely miscible blend [11]. PVA/PAA is, therefore, commonly used for producing wound

* Corresponding author.
E-mail address: mnugent@ait.ie (M. Nugent).

https://doi.org/10.1016/j.mtchem.2021.100549

dressings [12], adsorbents for wastewater treatment [13], solid polymer electrolytes for alkaline batteries and other electrochemical systems [14]. Although the combination of PVA and PAA nanofibres via electrospinning have been extensively studied [12,15–18], the concept of producing bilayer electrospun nanofibres with PVA and PAA is of potential interest in the synthesis of novel hydrogel-based nanofibres. Moreover, the PVA/PAA bilayer hydrogels were investigated before [19–21] but not in the form of polymeric nanofibres.

Our group has previously produced a bilayer hydrogel consisting of PVA and PAA on a macroscale, in which we demonstrated that both physical crosslinks between two different hydrogels compositions occur after freeze-thawing, resulting in double the theophylline drug-releasing time from the bilayer PVA/PAA hydrogel with a high molecular weight of PAA within 4 h compared with the PVA single layer hydrogel [22]. Further research in this study has allowed us to optimize the assembly of PVA/PAA bilayer hydrogel in nanoscale using electrospinning with the potential to be used for dual drug delivery applications. Researchers have already produced bilayer electrospun nanofibres with different polymers for either single or dual drug delivery. For example, bilayer poly (lactic-co-glycolic acid) (PLGA) scaffolds containing vascular endothelial growth factor (VEGF) and platelet-derived growth factor (PDGF) in separated layer revealed that the release of VEGF was faster than PDGF as the VEGF contained PLGA layer degraded faster than PDGF contained PLGA layer [23].

Previous works have highlighted the potential usage of a bilayer electrospun membrane for drug delivery and mechanical improvement of polymeric nanofibres [24–26]. Within these various studies, stands out the incorporation of microparticles loaded with drug, or nanofibres, within a bilayer which is further heat-annealed to assemble this membrane [27]. Moreover, studies have also shown that it is possible to use different polymers in this bilayer to present a hydrophobic and hydrophilic side to present a preferential drug release, particularly in the hydrophilic facet [28]. However, the study of dual drug delivery using this technique was not yet thoroughly evaluated, particularly if these different hydrophobic-hydrophilic sides were incorporated with synergetic drugs to understand their potential improvement in the drug release.

Thermal treatment is proposed to be a viable method to enhance the tensile strength, thermal stability and water stability [29,30] of biomaterials due to the crystallization and crosslinking in the polymer matrix. As reported by Park et al. [17], the water stability of electrospun PVA/PAA nanofibres prepared by blending the PVA solution with the PAA solution at PAA weight fraction = 0.5 was dramatically enhanced through heat treatment with conserved fibrous morphology. However, the study of two distinct layers combining together (i.e. PVA/PAA bilayer) for drug delivery and tissue engineering has not been investigated yet.

Therefore, the unannealed and annealed PVA, PAA and PVA/PAA bilayer electrospun nanofibres prepared in this study were subjected to several tests, including field emission electron microscopy (FESEM), Fourier transform infrared spectroscopy (FTIR), differential scanning calorimetry (DSC), dynamic mechanical analysis (DMA), water contact angle, disintegration, swelling and weight loss studies. In this work, a doxorubicin drug was incorporated in this synthesized membrane to be used for osteosarcoma treatment. Previous works presented the effectiveness of using PVA microspheres for doxorubicin release [31], presenting high cytotoxicity against osteosarcoma cells [32]. To prove the effectiveness of a dual drug delivery system using this membrane, clarithromycin was added to, hypothetically, obtain a synergetic enhancement of doxorubicin efficacy. This was suggested because a recent work-related that this occurs for MCF7 cells, breast cancer cells [33].

2. Materials and methods

2.1. Materials

PVA (Mowiol® 56-98) with a molecular weight of 196,000 g/mol (98.0–98.8 mol% hydrolyzed) and PAA with a molecular weight of 450,000 g/mol were purchased from Sigma-Aldrich. Distilled water and 99% ethanol were used as the solvent in the sample preparation step. Doxorubicin (DOX) hydrochloride was purchased from Cayman Chemical Company, and Clarithromycin was purchased from Tokyo Chemical Industry Co. Ltd. The U2OS human osteosarcoma cell line was kindly provided by the Genome Stability Lab of the National University of Ireland Galway.

2.2. Polymer solution preparation

PVA and PAA polymeric solutions were prepared using solvents as illustrated in Fig. 1. For PVA polymeric solution, 10 %w/v was prepared using distilled water and heated at 70 °C with stirring for 1.5 h. When the PVA solution was completely dissolved, ethanol was further added into the PVA solution with a ratio of 50:50 to achieve a final concentration of 5 %w/v. The solution was further stirred for 1 h at 45 °C to prevent ethanol evaporation and produce a homogeneous solution. Then, 3 %w/v PAA solution was prepared using ethanol and stirred for 2 h without heating.

2.3. Electrospun nanofibres preparation

A horizontal electrospinning machine (Spraybase®, Ireland) was used to produce the electrospun nanofibres. Each polymeric solution was poured into a 15 ml centrifuge plastic test tube and placed inside a pressure vessel that was connected to a blunt 20 G needle via a polytetrafluoroethylene (PTFE) tube. The tip of the needle was mounted at 13.5 cm vertically above a stainless-steel plate. The PVA was prepared using a voltage of 8.0 ± 0.5 kV. Conversely, the PAA nanofibres were prepared using a voltage of 10 ± 0.5 kV. Each polymeric solution was electrospun for 2 h. To prepare the PVA/PAA bilayer nanofibres, PAA nanofibres were directly spun onto the top of the PVA nanofibres layer.

2.4. Thermal annealing applied on electrospun nanofibres

The electrospun nanofibres samples (i.e. PVA, PAA and PVA/PAA bilayer) were annealed at two different temperatures, one batch at 150 °C for 40 min and another batch at 100 °C for 3 h in an oven. During the annealing process, no force was applied on the samples.

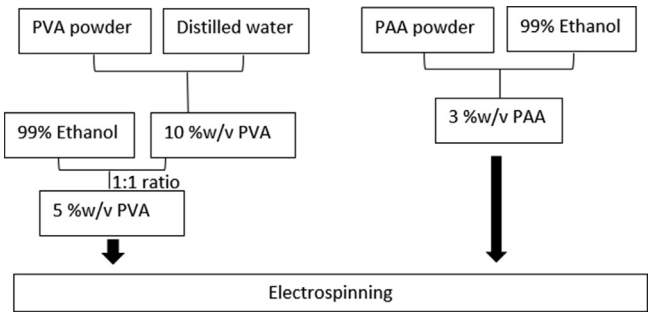

Fig. 1. Schematic diagram of the preparation of polyvinyl alcohol/polyacrylic acid bilayer nanofibres.

2.5. Sample characterization

2.5.1. FESEM

The surface and cross-section morphology of electrospun samples was observed using a FESEM (TESCAN, model MIRA 3). The diameter of the nanofibres was measured by taking 40 random readings from each sample using ImageJ software to get the mean value. The average thickness of the PVA/PAA bilayer nanofibres was measured by taking 10 random readings at different locations of the cross-section on the same image. In addition, the physical integrity behavior was examined from the changes of fibrous morphologies after swelling in pH 7.4 buffer.

2.5.2. FTIR

FTIR (PerkinElmer Spectrum One) was used to examine the chemical structure of PVA and PAA. The IR spectra were recorded in the spectral range of 500–4,000 cm^{-1}, and the absorption bands were identified using Spekwin32 spectroscopy software.

2.5.3. DSC

A DSC2920 Modulated DSC (TA Instruments, Inc.) was used to perform the thermal analysis. A heating rate of 5 °C/min under the flow of nitrogen gas was applied to each sample. The samples were tested in 3 cycles (heating-cooling-heating cycle). In the first cycle, the sample was heated from 25 °C to 280 °C. In the second cycle, the sample was cooled in the furnace to 25 °C. In the third cycle, the sample was re-heated from 25 °C to 280 °C. The degree of crystallinity, X_c of the samples was determined from the endothermic area using the following equation:

$$X_c = \frac{\Delta H_f}{\Delta Hf_o}$$

where ΔH_f is the measured enthalpy of fusion of the PVA sample and ΔH_{fo} is the thermodynamic enthalpy of fusion for 100% crystalline PVA ($\Delta H_{fo} = 138.60$ J/g) [34].

2.5.4. DMA

The nanofibre samples (15 × 8 mm) were analyzed using a TA Instrument Q800 DMA in a tension mode. They were tested at a 5 °C/min heating rate under a nitrogen atmosphere with 1 Hz frequency and 0.1 N pre-load force. The temperature sweeps in a range of 25 °C–160 °C.

2.5.5. Water contact angle

A contact angle system (FTA 1000 Analyzer System, First Ten Angstroms Inc., USA) was used to measure the contact angle of the specimen surface. A small drop of distilled water was placed onto the dry specimen surface, and the contact angle was recorded at 27 s. The test was carried out in a quadruplicate for each sample. A material is considered hydrophilic when the water contact angle is lower than 90°.

2.5.6. Swelling and weight loss studies

The unannealed and annealed PVA, PAA and PVA/PAA nanofibre samples were immersed in 10 ml pH 7.4 buffer at room temperature and the weight of the wet sample was measured at a specific time interval up to 24 h. The swelling index was calculated using the following equation:

$$Swelling\ index = \frac{W_t - W_0}{W_o} \times 100$$

where W_t is the weight of swollen sample at specific time, W_o is the weight of dry sample. The experiment was done in triplicate.

The weight loss was studied to examine the water stability of the nanofibre samples. The weight of dried samples was measured before being immersed in 10 ml of pH 7.4 buffer at room temperature for 24 h. After that, the swollen samples were placed on soft paper to remove surface water and rinsed with distilled water to remove residual buffer salts. The wet samples were then dried in an oven at 37 °C until a constant weight was achieved. The experiment was carried out in duplicate.

2.5.7. Disintegration test

The unannealed and annealed PVA, PAA and PVA/PAA nanofibre samples (1 cm × 1 cm) were immersed in 5 ml of pH 7.4 buffer at room temperature. The appearance of samples was then observed at 0, 24 and 48 h.

2.5.8. In vitro drug dissolution study

DOX hydrochloride and clarithromycin (CLA) were used as the model drug to evaluate the drug release profile of bilayer PVA/PAA nanofibres. 1.5 mg/ml of DOX was incorporated into the PVA solution before electrospinning, and this was labeled as PVA/DOX. While, two concentrations (2,000 μM and 500 μM) of CLA were incorporated into separate PAA solutions before electrospinning. The PAA solution that contained 2,000 μM CLA was labeled as PAA/CLA high, while the PAA solution that contained 500 μM CLA was labeled as PAA/CLA low.

The drug dissolution study was conducted using the rotating basket method at a speed of 100 rpm. The nanofibre samples were placed in 450 ml of phosphate buffer pH 6.5 at 37 °C. 2 ml of sample were collected at specific time points, and 2 ml of fresh buffer was replaced after each time of sample removal to maintain the sink condition. The amount of drug released was determined at the wavelength of 485 nm and 205 nm for DOX hydrochloride and clarithromycin, respectively, using a UV/Vis Spectrophotometer (Shimadzu Spectrophotometer UV-1280).

2.5.9. In vitro cytotoxicity test

The U2OS human osteosarcoma cell line was cultured in McCoy's 5A medium, supplemented with 10% FBS, 100 U/ml penicillin and 100 μg/ml streptomycin at 37 °C in an incubator containing 5% CO_2. U2OS cells (1×10^4 cells/well) were seeded in 96-well plate and incubated for 48 h. The cells were then treated with pure PVA and PAA nanofibres (positive controls) and nanofibres contained DOX or/and CLA for 24 h. After the treatment, the culture medium was removed and replaced by 200 μl/well fresh medium with 20 μl/well MTT reagent (5 mg/ml). The plates were then incubated for 3 h at 37 °C. After this period, the medium was removed and 200 μl/well DMSO was added for 1 h. The optical density was recorded at 550 nm in a microplate reader (BioTek Synergy HT, Swindon, UK), and the percentage of cell viability was determined.

Based on the MTT results, the coefficient of drug interaction (CDI) was calculated to analyze the effects of drug combinations. The CDI value was determined as follows: CDI = AB/(A × B) [35,36], where AB being the ratio of the drug association group (i.e. DOX + CLA) to the control group, and A or B are the ratios of the single drug group (i.e. DOX or CLA) to the control group. The CDI values of 1, <1 or >1 express additive, synergistic or antagonistic effects, respectively. CDI value < 0.7 demonstrates a strong synergism of the drug association.

2.5.10. Statistical analysis

The statistical analysis was performed using Prism 5 GraphPad software (La Jolla, CA, USA). Statistics for the water contact angle study was performed using Two-way ANOVA followed by a Dunnett's multiple comparisons test. For the statistical analysis of the

average diameter of nanofibres, One-way ANOVA followed by Tukey test was performed.

A p-value less than 0.05 was considered to be statistically significant. In all cases * was used for $p < 0.05$, ** for $p < 0.01$, and *** for $p < 0.001$, and **** for $p < 0.0001$. All experiments were performed at least in triplicates. Data were presented as mean ± SD for each result.

3. Results and discussion

3.1. The thermal annealing temperature and time

The prepared PVA/PAA bilayer electrospun nanofibres were physically crosslinked through thermal annealing. The crosslinking effectiveness of the PVA/PAA nanofibres can be influenced by annealing depending on the temperature [37], length of annealing time and the molecular weight of PAA or PVA [38]. Fig. 2 exhibits a visual macroscopic observation of the nanofibres prepared at different annealing temperatures and annealing times. The electrospun nanofibres were decomposed from white to slightly yellowish color (Fig. 2i) at 150 °C. Furthermore, the sample became hard and crispy. In fact, the degraded nanofibre showed a brownish or yellowish color [38]. Therefore, nanofibre samples annealed at 150 °C with mild degradation were not tested in the study.

Nanofibre samples annealed at 100 °C for 3 h (Fig. 2ii), also demonstrated by Zeng et al. [38], retained the same color before annealing (Fig. 2iii), which was white with no degradation were subjected for further analysis. Although the nanofibres annealed at 100 °C were slightly transparent when compared to the unannealed nanofibres, both their structure remained to be flexible.

3.2. FESEM results

As shown in Fig. 2a–d, the PVA nanofibres and PAA nanofibres in PVA/PAA bilayer nanofibres were randomly aligned. PVA solutions are normally prepared using distilled water. However, production of ultrafine nanofibres using water as a solvent is hardly achievable because of its low conductivity and high surface tension of water, which requires high voltage to obtain a stable jet and it might exceed the electric breakdown threshold of the surrounding gaseous medium, air in such cases, producing a corona discharge [39]. Therefore, it is important to be aware that the content of ethanol presented in polymer solutions could lower the surface tension and form a stable Taylor cone that gradually modifies the morphology of nanofibres from beaded nanofibres to ultrafine nanofibres [40]. As reported by Zhang et al. [41], the ethanol/water ratio of less than 5:95 in PVA solution can speed up the solvent evaporation rate as the jet travel through the air and what is reached through the collector is only smooth nanofibres. In our work, the ethanol/water ratio was increased up to a 50:50 ratio, the formation of non-beaded nanofibres was achieved and yet the diameter of nanofibres was not uniform. The addition of a high amount of ethanol has heavily decreased the surface tension of the electrospinning solutions, which led to the unstable liquid jet formation and non-uniform fiber size.

Interestingly, the FESEM images revealed changes in the diameter of PVA and PAA nanofibres, as well as the thickness of the PVA/PAA bilayer after the thermal annealing process. Before annealing, the average diameter of PVA nanofibres (Fig. 2a) and PAA nanofibres (Fig. 2c) was 341 ± 220 nm and 437 ± 188 nm, respectively. After annealing, the average diameter of PVA nanofibres (Fig. 2b) and PAA nanofibres (Fig. 2d) was increased to 464 ± 152 nm and 611 ± 166 nm, respectively. There is no significant difference between unannealed PVA nanofibres and annealed PVA nanofibres, while there is a significant difference ($p < 0.001$) between unannealed PAA nanofibres and annealed PAA nanofibres. It is suggested that the diameter of nanofibres increased because of the nanofibres released stress during heating and caused the polymer chains to orientate in axial, followed by expanding in the horizontal direction. It is possible that the thinnest fibers may present a different behavior when under annealing because it surpasses the glass transition of the polymer. Therefore, it is possible that agglomeration of finer fiber occurred. Nonetheless, these values were not statistically significantly different between annealed and non-

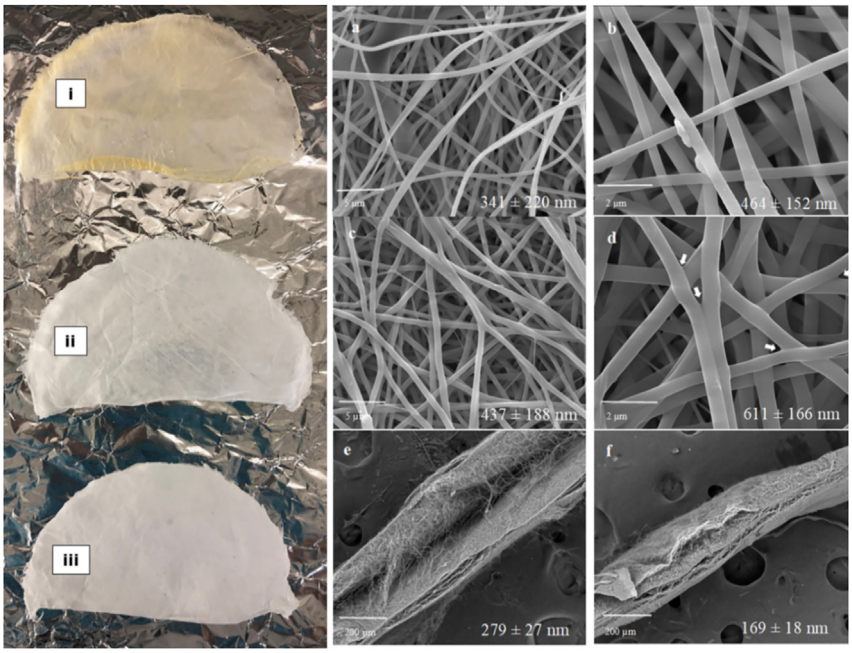

Fig. 2. PVA nanofibre sample annealed (i) at 150 °C with slightly degradation, (ii) at 100 °C and (iii) unannealed. Surface morphology of (**a**) Unannealed PVA/PAA bilayer (PVA surface), (**b**) Annealed PVA/PAA bilayer (PVA surface), (**c**) Unannealed PVA/PAA bilayer (PAA surface), and (**d**) Annealed PVA/PAA bilayer (PAA surface). The cross-section morphology of (**e**) Unannealed PVA/PAA bilayer and (**f**) Annealed PVA/PAA bilayer. PAA, polyacrylic acid; PVA, polyvinyl alcohol.

annealed. Previous works also reported an increase in diameter of the annealed poly (vinyl pyrrolidone) (PVP) nanofibres when a slow heating rate (i.e. 1, 3, 4 °C/min) is performed, which was attributed to the nucleation process [42,43].

In contrast, as seen on the cross-section morphology of the PVA/PAA bilayer nanofibres, the thickness of the PVA/PAA bilayer nanofibres decreased after annealing, with the thickness of 279 ± 27 μm and 169 ± 18 μm for the unannealed (Fig. 2e) and annealed PVA/PAA bilayer (Fig. 2f), respectively. The annealed bilayer nanofibres were remained to be two discrete layers and yet the two layers were 'glued' together, leaving fewer spaces between the nanofibre layers. Moreover, the thermal annealing induced the *in situ* fiber-fiber fusion (interfibre bonding) [44]. This fusion can be observed by looking at the sharp vertex formed by overlapped nanofibres which became rounded, as indicated by the arrows in Fig. 2d. Furthermore, the mechanical properties of nanofibres can be enhanced with an increase in interfibre bonding.

Fig. 3 showed the surface morphology of electrospun nanofibres after swollen in pH 7.4 buffer for 48 h. Although all the swollen nanofibres were destroyed, the annealed bilayer PVA/PAA nanofibres retained a porous structure, which is due to the heat-annealing treatment. The unannealed and annealed PAA nanofibres were completely dissolved after 48 h. Thus, there were no SEM images for swollen PAA nanofibres.

3.3. FTIR results

The major absorption bands of PVA and PAA were identified in the FTIR spectrum (Fig. 4). The characteristic peaks of unannealed and annealed PVA (Fig. 4a and b) which included the peak around 3,290 cm^{-1} for O–H stretching, 2,943 and 2,911 cm^{-1} for C–H stretching of the alkyl group, 1,431 cm^{-1} for C–H bending in CH_2 groups, 1,266 cm^{-1} for C–O stretching, 1,141 cm^{-1} for C–O–C stretching, 1,092 cm^{-1} for C–O stretching, 920 cm^{-1} for C–H stretching and 838 cm^{-1} for C–C stretching [45]. When comparing unannealed PVA with annealed PVA, there was an extra peak at 1,141 cm^{-1} on the annealed PVA spectra, which represented the crystalline sensitive band [46]. The PVA crystallization is caused by the thermal annealing treatment.

Furthermore, the major absorption bands of unannealed and annealed PAA (Fig. 4e and f) included the peaks around 3,506 cm^{-1} for free O–H group, 3,138 cm^{-1} for bonded O–H group, 2,943 cm^{-1}

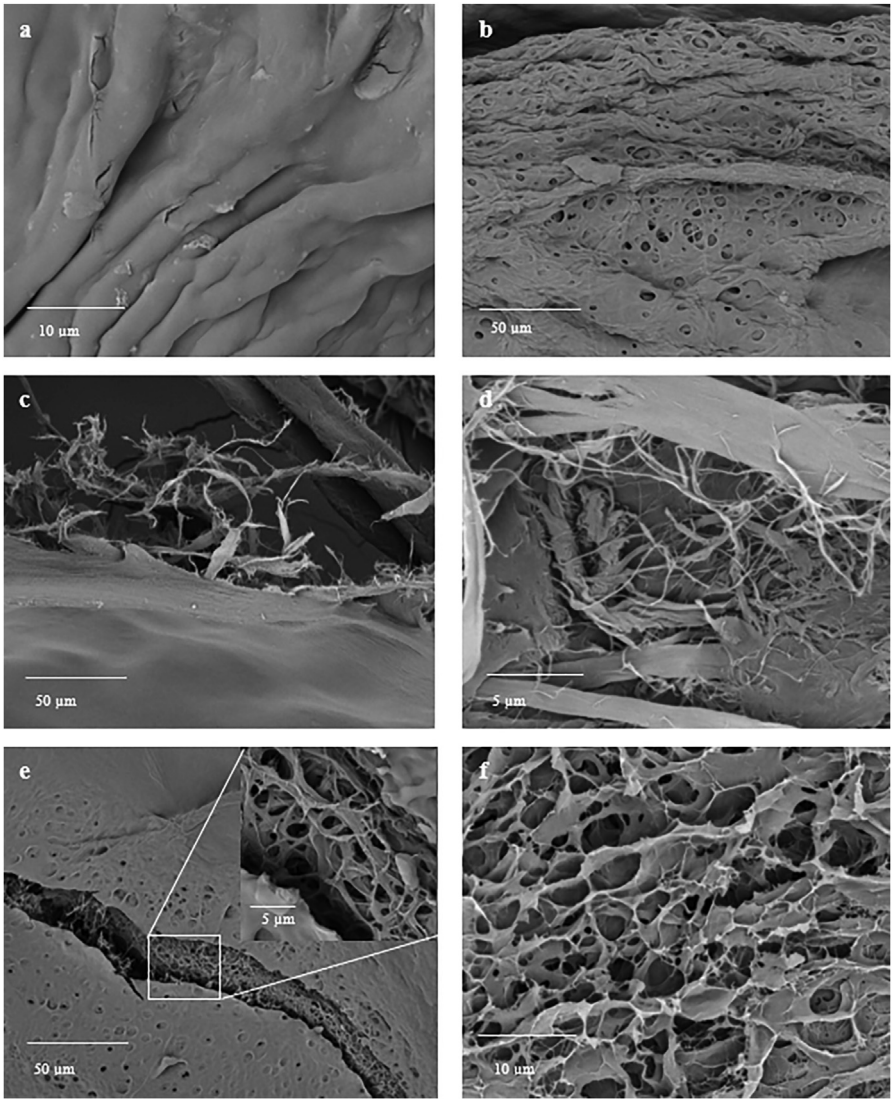

Fig. 3. Electrospun nanofibres after swollen in pH 7.4 buffer for 48 h, (**a**) Unannealed PVA, (**b**) Annealed PVA, (**c**) Unannealed PVA/PAA bilayer (PVA surface), (**d**) Unannealed PVA/PAA bilayer (PAA surface), (**e**) Annealed PVA/PAA bilayer (PVA surface) and (**f**) Annealed PVA/PAA bilayer (PAA surface). PAA, polyacrylic acid; PVA, polyvinyl alcohol.

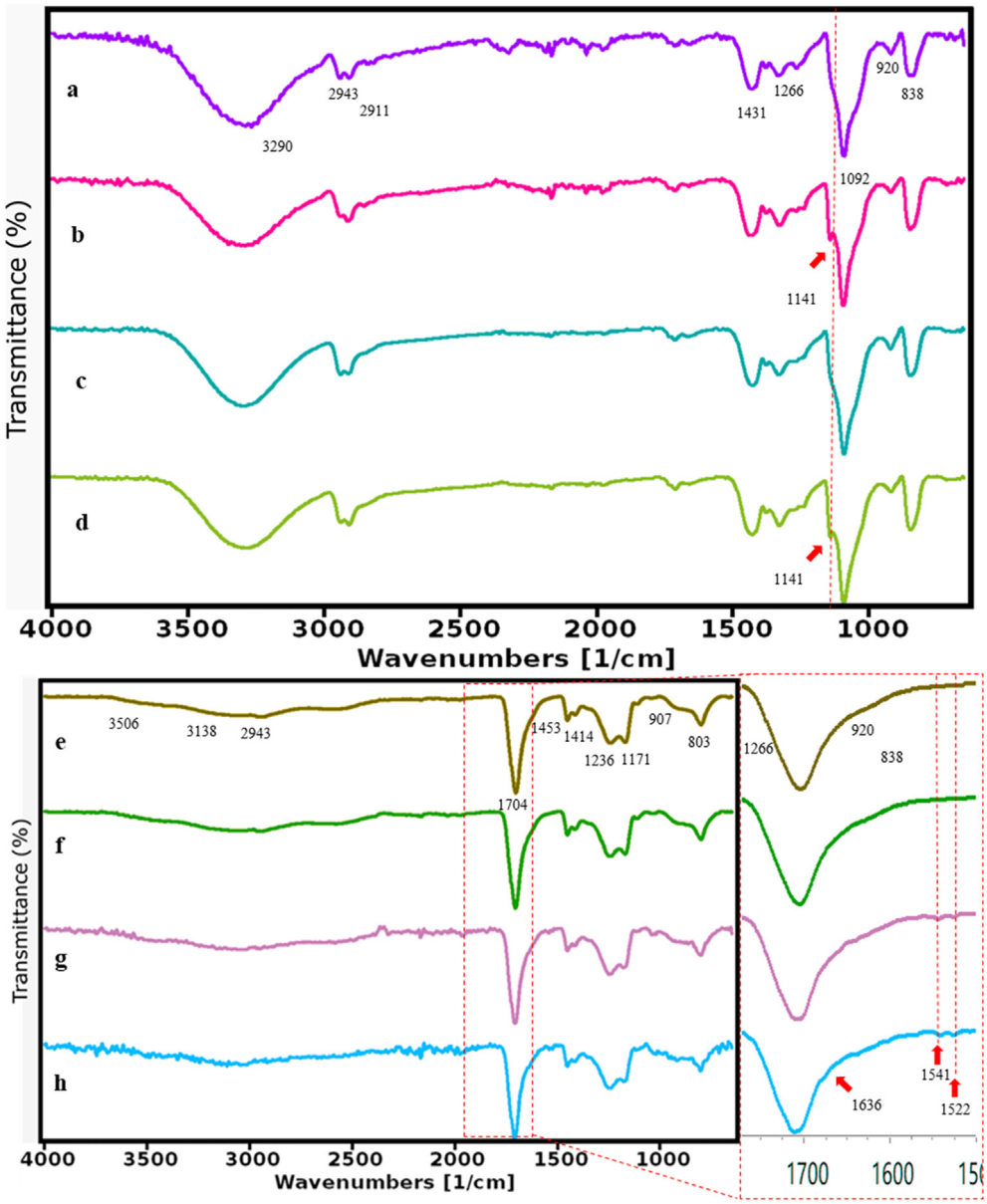

Fig. 4. FTIR result of the electrospun nanofibres: (**a**) Unannealed PVA, (**b**) Annealed PVA, (**c**) Unannealed PVA/PAA (PVA surface), (**d**) Annealed PVA/PAA (PVA surface), (**e**) Unannealed PAA, (**f**) Annealed PAA, (**g**) Unannealed PVA/PAA (PAA surface), (**h**) Annealed PVA/PAA (PAA surface). PAA, polyacrylic acid; PVA, polyvinyl alcohol.

for C–H stretching, 1,704 cm^{-1} for C=O stretching of carbonyl group, 1,453 cm^{-1} for C–H bending in CH_2 groups, 1,414 cm^{-1} for C–O–H bending, 1,236 cm^{-1} for C–O stretching, 1,171 cm^{-1} for C–O stretching, 907 cm^{-1} for C–O symmetric stretching and 803 cm^{-1} for CH_2 rocking [47,48].

It is very difficult to identify the overlapping of PVA and PAA dominant peaks on the obtained spectra of the unannealed and annealed PVA/PAA bilayer nanofibres. This might be due to the bilayer nanofibres being too thick to determine the dominant peaks of the PAA surface when testing the PVA surface or vice versa. It can be concluded that the PVA and PAA did not completely blend together after annealing, two discrete layers still remained. Therefore, both PVA surface and PAA surface of the unannealed and annealed PVA/PAA bilayer nanofibres were analyzed separately.

On the PVA surface of the PVA/PAA bilayer, the degree of PVA crystallinity in the annealed PVA/PAA bilayer nanofibres (Fig. 4d) has increased when compared with the unannealed PVA/PAA bilayer (Fig. 4c). It is supported by the sharper peak at 1,141 cm^{-1} assigned to C–O–C stretching and C–C stretching. This result is similar to the result obtained from pure PVA nanofibres spectra.

It is possible that an esterification occurred from ester cross-linking, with presence of hydroxyl groups (–OH) of PVA molecules and carboxyl groups (C=O) from PAA molecules as previously reported [19]. On the PAA surface of the PVA/PAA bilayer, the peaks at 1,522 cm^{-1} and 1,541 cm^{-1} (as indicated by the red region) were observed on both unannealed (Fig. 4g) and annealed (Fig. 4h) PVA/PAA bilayer, suggesting a shift peak from the band of 1,610–1,560 cm^{-1} assigned to $-COO^-$ [49]. Moreover, the annealed

PVA/PAA bilayer (Fig. 4h) showed a peak at 1,636 cm^{-1} (as indicated by the red region) assigned to C═O from ester crosslinking [50].

3.4. DSC results

The glass transition temperature (Tg) and melting temperature (Tm) of the pure PVA, pure PAA and PVA/PAA bilayer nanofibres before and after annealing were identified from the DSC thermographs and illustrated in Fig. 5a. As reported by Samprasit et al. [51], the absence of endothermic and exothermic peaks below 100 °C indicates the low moisture contents of the substances. Therefore, the endothermic peaks observed in the temperature range of 41–53 °C attributed to the evaporation of adsorbed water in the samples [52]. Moreover, all the heat flow curves upon the cooling cycle and second heating cycle of each sample were a flat shape (Supplementary material S.1). The flat shape was caused by the rupture of ionic clusters of the sample around 250 °C at the first heating cycle, and hence, the polymer morphology is no longer possible to be recovered [53]. Therefore, the Tg and Tm of each sample were determined on the first heating cycle.

The Tg values decreased significantly from 132 °C to 86 °C in pure PVA nanofibres after annealing. It might be due to annealing, caused by the relaxation of polymer chains and rearranged the crystallites into a crystal lattice, an effect seen for annealed starch [54]. In contrast, the Tg of pure PAA nanofibres increased from 102 °C to 120 °C after annealing because of the formation of strong covalent bonds in the anhydrides attributed by crosslinking that limited the segmental motions of the polymer chains [55]. In contrast to the pure PVA nanofibres, the Tg was not affected in the PVA/PAA bilayer nanofibres, the Tg was between 119 °C and 121 °C.

The endothermic melting peak of unannealed and annealed pure PVA were around 222 °C–223 °C and the crystallinity increased from 45% to 75% after annealing. While the pure PAA nanofibres showed no melting peak because it is amorphous [56]. For the unannealed and annealed PVA/PAA bilayer nanofibres, the Tm was the same at 221 °C. The PVA/PAA bilayer nanofibres had 27% and 30% crystallinity before and after annealing, respectively. This is similar to the result of Chen et al. [29], annealing promoted the formation of crystallites of the PVA/PAA nanofibres.

3.5. DMA

The dynamic of the glass transition temperature in nanofibres samples was remeasured using DMA as the sensitivity of DMA is higher than that of DSC. As illustrated in Fig. 5b, the Tg of unannealed pure PVA nanofibres was 110 °C. The annealed pure PVA nanofibres exhibited two peaks at 84 °C and 131 °C. The first peak at 84 °C is called the α_a relaxation peak, and it represents the glass transition temperature; the second peak at 131 °C is called the β_c relaxation peak, it is due to the relaxation in the PVA crystalline domains [57]. The results for pure PVA nanofibre samples were similar to DSC.

Furthermore, as illustrated in Fig. 5c, the Tg of unannealed and annealed pure PAA nanofibres was found around 135 °C and 134 °C, respectively. The results were similar to the result reported by Garza et al., the centrifugally spun PAA nanofibres were found to have a Tg at 135.73 °C in DSC analysis [58]. By looking at the tan delta curve, there was a large drop after Tg in the pure PAA nanofibres, this might be due to the large shift of polymer chains and dehydration of adjacent carboxylic groups for anhydrides formation [58].

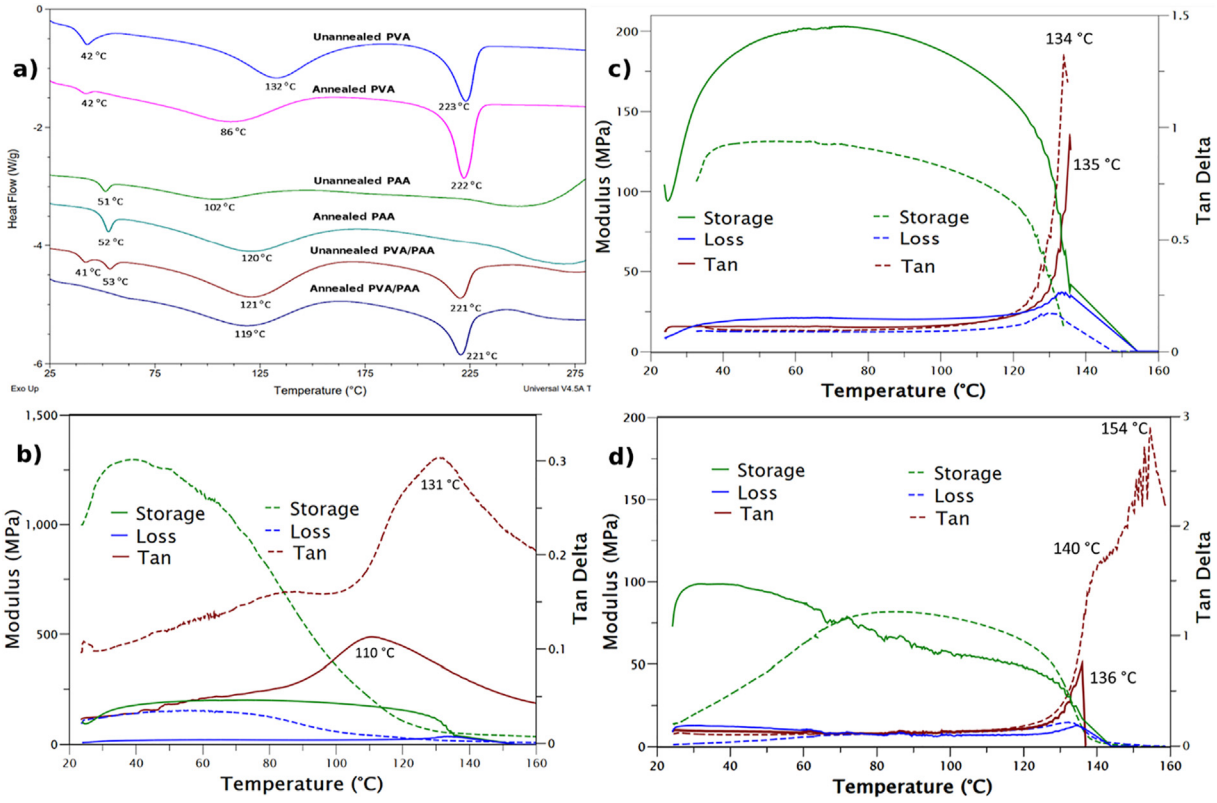

Fig. 5. (**a**) DSC thermographs of the nanofibre samples. DMA spectra for (**b**) PVA, (**c**) PAA and (**d**) PVA/PAA bilayer nanofibre samples (Solid line represented unannealed samples; dashed line represented annealed samples). DMA, dynamic mechanical analysis; DSC, differential scanning calorimetry; PAA, polyacrylic acid; PVA, polyvinyl alcohol.

As seen in Fig. 5d, the unannealed PVA/PAA bilayer nanofibre sample has the Tg around 136 °C. A sudden drop of Tan delta to 0 was observed after Tg, suggested the transition of the glassy region to the fluid region was increased for the unannealed PVA/PAA bilayer nanofibre sample. While the annealed PVA/PAA bilayer nanofibres sample has a Tg at 140 °C, and a βc relaxation peak at 154 °C. Therefore, the crosslinking reaction increased the Tg values of samples annealed characteristic of ester linkage and provided an improved mechanical property to these samples.

The variation of storage modulus in term of elasticity of PVA, PAA and PVA/PAA bilayer nanofibres are also determined using DMA. The unannealed PVA nanofibres has a storage modulus of ~219 MPa. After annealing, the PVA nanofibres showed the highest storage modulus at ~1,380 MPa. It is directly related to the degree of crosslinking. Thus, the annealed PVA nanofibres has the highest degree of crosslinking, which supported by the DSC result. The storage modulus of unannealed and annealed PAA nanofibres are ~200 MP and ~132 MPa, respectively. Moreover, the unannealed and annealed PVA/PAA bilayer nanofibres have the lowest values of storage modulus of ~95 MPa and ~87 MPa, respectively. Due to the presence of PAA in the bilayer nanofibres, the storage modulus decreased, the stiffness of the materials decreased.

3.6. Water contact angle

The water contact angle is the most straightforward method to measure the wettability property of a solid surface. The hydrophilicity increases with a lower water contact angle. The PVA/PAA bilayer nanofibres are produced by a layer of pure PVA nanofibres and a layer of pure PAA nanofibres. It is proposed that the PVA and PAA were not melted and formed a blend after thermal annealing. As illustrated in Fig. 2, the annealed bilayer nanofibres sample still remained as two discrete layers. Therefore, the hydrophilicity was tested on both surfaces (i.e. PVA surface and PAA surface) of the PVA/PAA bilayer nanofibres.

Fig. 6 shows that the surface wettability of PAA nanofibres was better than PVA nanofibres. On the PVA/PAA bilayer nanofibres, it can be seen that the contact angles of the PAA surface (unannealed: 0°; annealed: 23°) were lower than the PVA surface (unannealed: 51°; annealed: 67°). This indicated the PVA/PAA bilayer nanofibres were more hydrophilic when the water contacted the PAA surface of the bilayer nanofibres. Moreover, the unannealed samples displayed a higher degree of hydrophilicity than the annealed samples. The PAA surface of unannealed PVA/PAA nanofibres demonstrated a vanishing contact angle $\theta = 0°$ within 27 s, indicating a super-hydrophilic wetting behavior, which can be attested to the hydrophilic group (C═O group). It can be concluded that the degree of hydrophilicity is related to the thermal annealing treatment and also depends on the type of polymers, in this case, both PVA and PAA.

In addition, it is observed that the PVA surface of the bilayer nanofibre has the highest contact angle (67°) after annealing, suggesting a significant decrease in hydrophilicity of the corresponding surface of PVA from the PVA/PAA bilayer nanofibres. An increase water stability of annealed PVA/PAA bilayer nanofibres could be caused by the increase in average diameter of nanofibres after annealing. Furthermore, it could be caused by the formation of hydrophobic ester groups within the PVA and PAA molecules and the physical crosslinking network among small crystals of PVA during annealing process [30,38,59].

Overall, there are significant difference of these samples (i.e. unannealed PAA ($p < 0.0001$), annealed PAA ($p < 0.0001$), annealed PVA/PAA bilayer (PVA surface) ($p < 0.01$), unannealed PVA/PAA bilayer (PAA surface) ($p < 0.0001$), annealed PVA/PAA bilayer (PAA

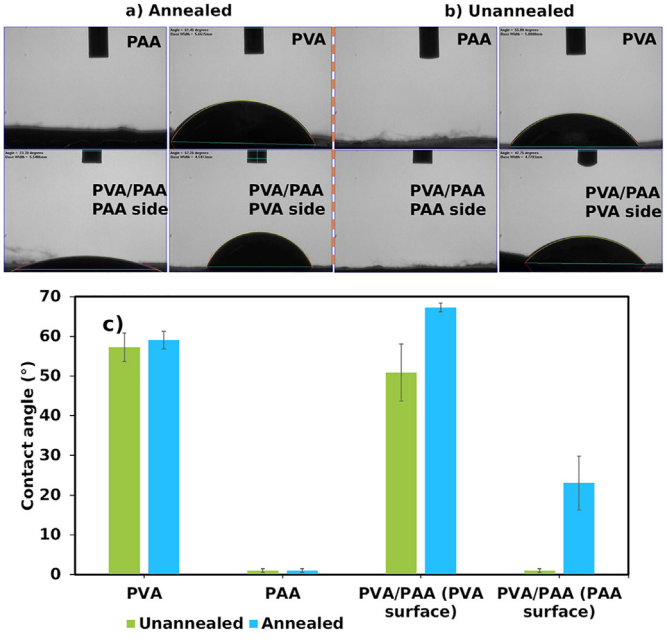

Fig. 6. Images of water droplet on (**a**) annealed nanofibre samples, and (**b**) unannealed nanofibre samples at 27 s. (**c**) Contact angle measurement of electrospun nanofibre samples.

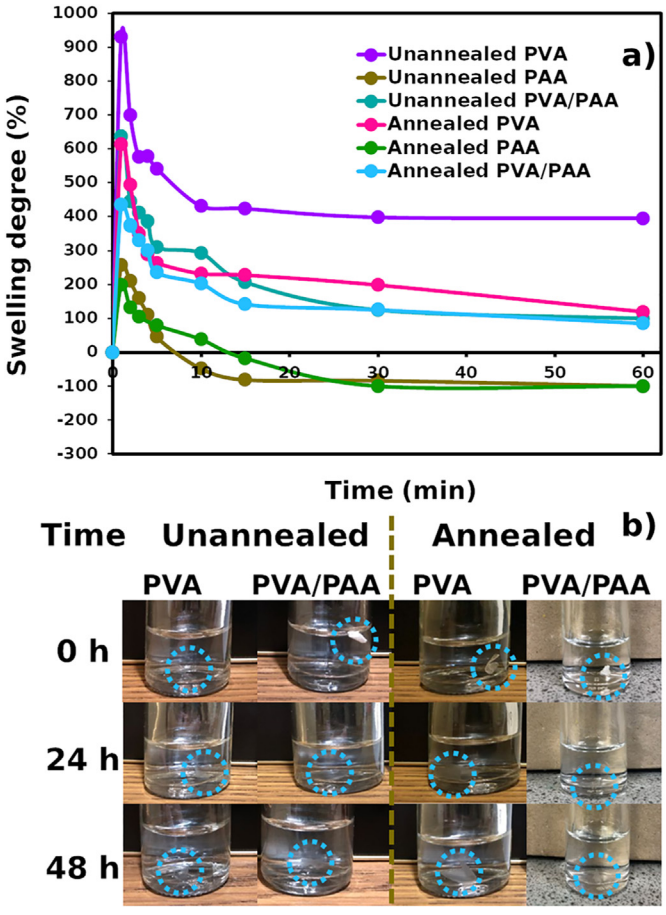

Fig. 7. (**a**) Swelling and degradation characteristic of unannealed and annealed PVA, PAA and PVA/PAA bilayer nanofibres. (**b**) Disintegration studies. PAA, polyacrylic acid; PVA, polyvinyl alcohol.

surface) ($p < 0.0001$)) when comparing with the unannealed PVA nanofibres.

3.7. Swelling and weight loss studies

As shown in Fig. 7b, the nanofibres have a very fast swelling rate, all the samples have achieved full swelling within 1 min and reached the plateau in 60 min. The unannealed PVA, PAA and PVA/PAA bilayer nanofibres have a maximum swelling degree of 930%, 257% and 637%, respectively. Furthermore, the results showed a lower swelling ratio in the annealed samples. The annealed PVA, PAA and PVA/PAA bilayer nanofibre samples have a maximum swelling degree of 613%, 199% and 437%, respectively. For pure PVA nanofibres, such a decrease of the swelling degree after thermal annealing treatment is influenced by the increase of PVA crosslinking density, i.e. the decrease of the polymer network free volume and subsequently decreased the polymer to swell in the buffer. For PVA/PAA bilayer nanofibres, PAA is used as a crosslinking agent and esterification crosslinking occurred during thermal annealing treatment. The decrease in swelling ratio of annealed PVA/PAA sample is expected to influence by the presence of PAA, indicating the crosslinking density was further increased by the esterification reaction [19,59].

It should be also taken into account that thermal annealing influences the hydrophilicity of the nanofibres (Fig. 6), and, consequently, contributes to the swelling ability of the nanofibres [60]. After the nanofibres were fully hydrated, the swelling index started to decrease because of the disintegration of nanofibres into the pH 7.4 buffer. The unannealed and annealed PVA and PVA/PAA nanofibres were partially disintegrated and reached equilibrium within 60 min. However, the unannealed and annealed PAA started to degrade at 7 min and 13 min, respectively (Fig. 7a). Although the annealing process did not improve the water stability of pure PAA nanofibres, the complete degradation of pure PAA nanofibres is extended from 15 min to 30 min.

Regarding the water stability of PVA/PAA bilayer nanofibres, owing to the high water solubility of PVA and PAA, the % weight loss of unannealed PVA and PVA/PAA bilayer nanofibres was 78% and 74%, respectively. However, after annealing, the % weight loss of annealed PVA and PVA/PAA bilayer nanofibres has decreased to 40% and 67%, respectively. The water stability of annealed PVA/PAA bilayer nanofibres was slightly improved. These swelling and degradation characteristics of nanofibres are of potential to modulate a complex dual delivery with two different poor solubility drugs on the bilayer nanofibres to improve the drug release profile.

3.8. Disintegration test

Same sizes of unannealed and annealed PVA, PAA and PVA/PAA bilayer nanofibres were immersed in the pH 7.4 buffer. As seen in Fig. 7b, the nanofibres curled and shrunk once they contacted the buffer. The PVA and PVA/PAA nanofibres with and without annealing were not completely disintegrated after 48 h of buffer immersion at room temperature. In contrast, the unannealed and annealed PAA nanofibres were dissolved within 30 min as mentioned in the swelling test. Hence, the PAA nanofibre layer on the unannealed and annealed PVA/PAA bilayer nanofibres might be completely disintegrated and only the PVA nanofibre layer was left after 48 h.

3.9. In vitro drug release

The drug release of the antibiotic (CLA in Fig. 8a, as clarithromycin) is steadily released, achieving 100% after 24 h. When the bilayer is used for this drug, there seems to be a slow-release rate attributed to the crosslink between layers that better entrap this drug.

However, no significant variation is seen with heat-annealing in the release rate for pure PAA because this drug was incorporated into the PAA, and this polymer readily dissolves underwater; therefore, it is expected that the annealing would weakly affect this rate. It is also interesting to notice that, even though the PAA is readily dissolved, there is a slower drug release rate for annealed bilayer both for high and lower dosages of this drug. Because of the interaction between the polymer and the drug changed after heating and it forms an assemble structure, it is possible that the crosslink, evidenced by the FTIR section, retained part of the drug at the interface of both films, and this behavior occurred.

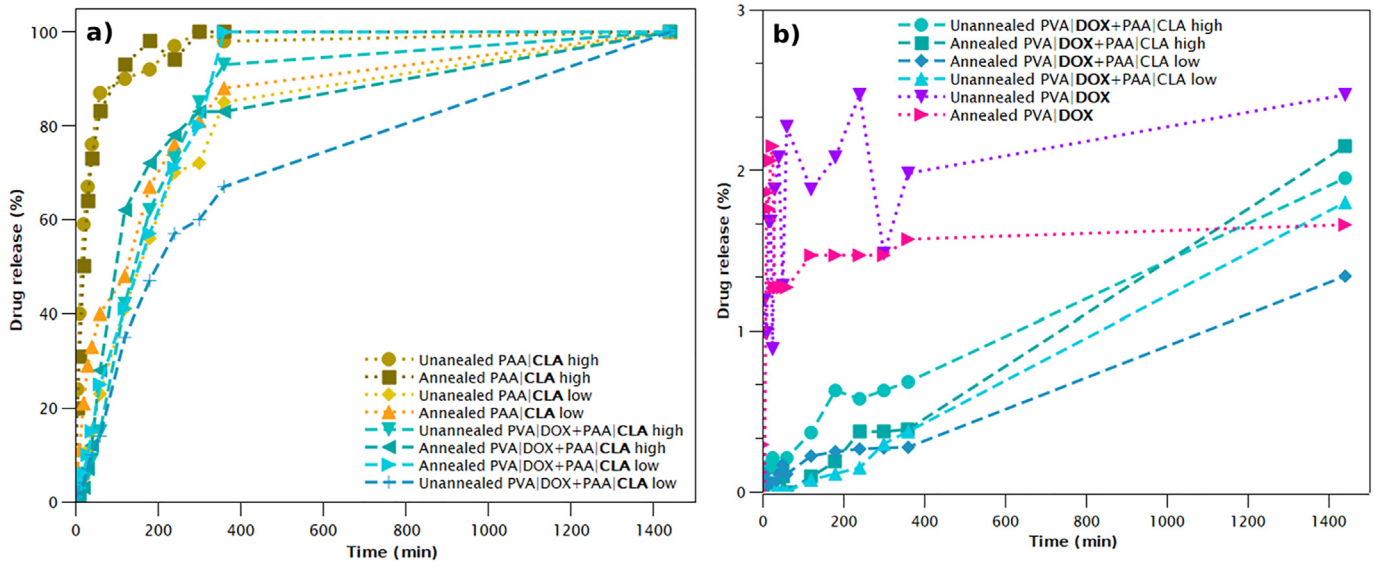

Fig. 8. Drug dissolution studies of (**a**) CLA and (**b**) DOX from the electrospun nanofibre samples. Bold character in the legend of each figure indicates the drug that is being studied. CLA, clarithromycin; DOX, doxorubicin.

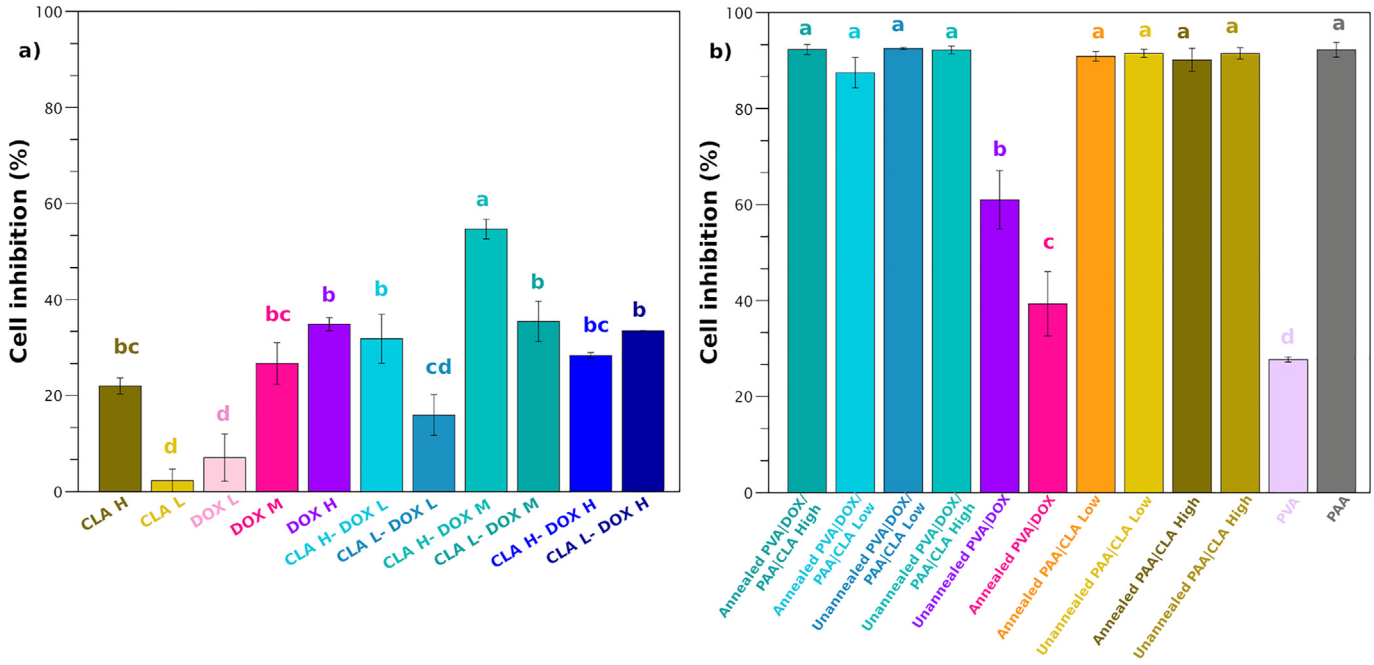

Fig. 9. Osteosarcoma U2OS cell cytotoxicity values against (**a**) pure and combined clarithromycin and doxorubicin effects at various dosages and (**b**) membrane loaded drugs. The specific concentration for each drug is described in supplementary material S.2 and S.3.

When doxorubicin is used, the pure PVA presents a very slow-release rate, and it further decreases with annealing (Fig. 8b). In addition, it seems that it reaches constant values after 24 h. Nonetheless, when a bilayer is used for releasing this drug, there seems to be a steady release rate, but it also reaches low maximum dosages at 24 h (2%). This is a very good indication that the drug will be slowly released with non-harmful dosages. Doxorubicin is very toxic, and controlling the rate of this drug is very important for any targeted application. Although, no further values after 24 h were made, it is possible that the drug will continue being delivered based on the profile of the release curve.

3.10. Cell inhibition studies

The human osteosarcoma U2OS cell line was used to investigate the effect of doxorubicin drug with or without CLA as it is reported that this antibiotic presents a synergism effect when used together with doxorubicin in MCF7 cells, breast cancer cells; therefore, we hypothesized that it also may present synergism against osteosarcoma cell line. Primarily the pure drugs of CLA and DOX were tested against the studied cells but also in conjunction using various dosages of both drugs. It can be seen in Fig. 9a that most concentrations slightly inhibit the cell growth with a mean of 30% (Supplementary material S.2), even the DOX dosages studied herein were not able to fully inhibit these cells. However, when both drugs are used in conjunction one specific dosage inhibited more than 55% while also statistically significantly different from all the other dosages. In this case, 0.374 mg/ml of CLA and 4 μg/ml of DOX. Regarding their synergism, CLA H-DOX M, CLA H-DOX L, CLA L-DOX L, CLA L-DOX M and CLA L-DOX H presenting a CDI value of 0.9, 0.9, 0.8, 0.8 and 0.9, respectively, indicating this specific dosages gave a synergism effect (CDI<1). Therefore, this result is rather unique because the combination of both drugs can also be used for the treatment of osteosarcoma.

When these drugs were incorporated into the electrospun membrane, their values further increased the cell inhibition from up to 90% (Fig. 9b); however, it is possible that these values may be masked by the PAA, which in this work indicates that it is extremely harmful to these cells. It is possible that the dissolution of the PAA creates an acidic environment, and the cells cannot proliferate, so the neutralization used for the pure PAA was inadequate. Nonetheless, membranes with pure DOX exhibited a decrease in cell inhibition when thermal treatment was performed, presenting a statistically significant difference, and this may be related to their drug release behavior where higher dosages were obtained with unannealed samples.

4. Conclusion

In summary, the PVA/PAA bilayer nanofibres were successfully prepared using electrospinning technology and thermal annealing treatment. Only the annealed nanofibres at 100 °C for 3 h without variation on the color tone from white, proving to be non-degraded nanofibres were analyzed. The morphology, diameter and thickness of the nanofibres samples were characterized by FESEM. The results showed an increase in the average diameter of annealed PVA and PAA nanofibres, but a decrease in thickness in annealed PVA/PAA bilayer nanofibres. Moreover, the crystallinity of the annealed PVA/PAA bilayer nanofibres has increased, indicating the increase of physical crosslinking within the PVA/PAA polymer matrix during the annealing process. The impact of PAA on the hydrophilic property of the PVA was described. There was a difference in the degree of hydrophilicity of the nanofibre surfaces of PVA and PAA. The PAA nanofibre layer had higher hydrophilicity than the PVA nanofibre layer. The annealed bilayer nanofibres can be considered as a potential to be used in modeling drug release especially for dual drug delivery, whereby biologically relevant drug molecules can be incorporated into the polymer solution before electrospinning. Further work would be useful to increase the crosslinking density by changing the temperatures and time of annealing. The combined effect of clarithromycin and doxorubicin proves that a synergetic enhance cytotoxicity against osteosarcoma cell line occurs and it may be improved with the bilayer electrospun bilayer. However, the PAA needs to be further evaluated for their safety of

usage. Nonetheless, a fast and slow release rate can be achieved using this membrane for any targeted application and this works provides the advantage of different surface hydrophilicity that could be modulated for the drug release rate of two different drugs on PVA/PAA bilayer nanofibres.

Credit author statement

Chee, B. S.: Methodology, Investigation, Validation, Formal analysis, Data curation, Writing – original draft, Writing – review & editing, Visualization. de Lima, G. G.: Methodology, Data curation, Writing – original draft, Writing – review & editing, Visualization. de Lima, T. A. M.: Methodology, Investigation, Validation, Data curation, Investigation. Seba, V.: Methodology, Investigation, Data curation, Lemarquis, C.: Investigation, Data curation. Pereira, B. L.: Formal analysis, Investigation. Bandeira, M.: Data curation, Investigation. Cao, Zhi.: Data curation, Investigation. Nugent, M. N..: Conceptualization, Methodology, Supervision, Funding acquisition, Project administration, Resources.

Data availability

The data used to support the findings of this study are included within the article.

Declaration of competing interest

The authors declare that they have no known competing financial interests or personal relationships that could have appeared to influence the work reported in this paper.

Acknowledgments

This work was supported by the Athlone Institute of Technology [President's Doctoral Scholarship]. Thank you Professor Janaina da Silva Crespo from Laboratório Central de Microscopia, Universidade de Caxias do Sul for the FESEM images.

Appendix A. Supplementary data

Supplementary data to this article can be found online at https://doi.org/10.1016/j.mtchem.2021.100549.

References

[1] J. Wang, V. Planz, B. Vukosavljevic, M. Windbergs, Multifunctional electrospun nanofibers for wound application – novel insights into the control of drug release and antimicrobial activity, Eur. J. Pharm. Biopharm. 129 (2018) 175–183, https://doi.org/10.1016/j.ejpb.2018.05.035.

[2] A.M. Al-Dhahebi, S.C.B. Gopinath, M.S.M. Saheed, Graphene impregnated electrospun nanofiber sensing materials: a comprehensive overview on bridging laboratory set-up to industry, Nano Converg. 7 (2020), https://doi.org/10.1186/s40580-020-00237-4.

[3] S.P. Sundaran, C.R. Reshmi, P. Sagitha, O. Manaf, A. Sujith, Multifunctional graphene oxide loaded nanofibrous membrane for removal of dyes and coliform from water, J. Environ. Manag. 240 (2019) 494–503, https://doi.org/10.1016/j.jenvman.2019.03.105.

[4] M. Arkoun, F. Daigle, R.A. Holley, M.C. Heuzey, A. Ajji, Chitosan-based nanofibers as bioactive meat packaging materials, Packag. Technol. Sci. 31 (2018) 185–195, https://doi.org/10.1002/pts.2366.

[5] L. Steffens, A.M. Morás, P.R. Arantes, K. Masterson, Z. Cao, M. Nugent, D.J. Moura, Electrospun PVA-Dacarbazine nanofibers as a novel nano brain-implant for treatment of glioblastoma: in silico and in vitro characterization, Eur. J. Pharmaceut. Sci. 143 (2020) 105183, https://doi.org/10.1016/j.ejps.2019.105183.

[6] L.S. Reinhardt, J.G. Henn, A.M. Morás, N.D. de Moura Sperotto, M.B. Ferro, Z. Cao, A.V. Roehe, A.U.S. Petry, M. Nugent, D.J. Moura, Plantago australis hydroethanolic extract-loaded formulations: promising dressings for wound healing, Rev. Bras. Farmacogn. 31 (2021) 91–101, https://doi.org/10.1007/s43450-021-00126-9.

[7] W.A. Laftah, S. Hashim, A.N. Ibrahim, Polymer hydrogels: a review, Polym. Plast. Technol. Eng. 50 (2011) 1475–1486, https://doi.org/10.1080/03602559.2011.593082.

[8] H.L. Lim, Y. Hwang, M. Kar, S. Varghese, Smart hydrogels as functional biomimetic systems, Biomater. Sci. 2 (2014) 603–618, https://doi.org/10.1039/c3bm60288e.

[9] G.G. de Lima, B.S. Chee, V.F. Moritz, Y.J. Cortese, W.L.E. Magalhães, D.M. Devine, M.J.D. Nugent, The production of a novel poly(vinyl alcohol) hydrogel cryogenic spheres for immediate release using a droplet system, Biomed. Phys. Eng. Express 5 (2019), 045017, https://doi.org/10.1088/2057-1976/ab2547.

[10] M. Rizwan, R. Yahya, A. Hassan, M. Yar, A.D. Azzahari, V. Selvanathan, F. Sonsudin, pH sensitive hydrogels in drug delivery : brief history , properties , swelling , and release mechanism , material selection and applications, Polymers (Basel) 9 (2017) 137, https://doi.org/10.3390/polym9040137.

[11] Q. Chena, H. Kurosub, L. Mab, M. Matsuo, Elongation-induced phase separation of poly(vinyl alcohol)/poly(acrylic-acid) blends as studied by 13 C CP/MAS NMR and wide-angle x-ray diffraction, Polymer (Guildf) 43 (2002) 1203–1206, https://doi.org/10.1016/S0032-3861(01)00690-5.

[12] H. Serinçay, S. Özkan, N. Yilmaz, S. Koçyiğit, I. Uslu, S. Gürcan, M. Arisoy, PVA/PAA-Based antibacterial wound dressing material with aloe vera, Polym. Plast. Technol. Eng. 52 (2013) 1308–1315, https://doi.org/10.1080/03602559.2013.814671.

[13] J.A. Park, J.K. Kang, S.C. Lee, S.B. Kim, Electrospun poly(acrylic acid)/poly(vinyl alcohol) nanofibrous adsorbents for Cu(ii) removal from industrial plating wastewater, RSC Adv. 7 (2017) 18075–18084, https://doi.org/10.1039/c7ra01362k.

[14] G.M. Wu, S.J. Lin, C.C. Yang, Preparation and characterization of PVA/PAA membranes for solid polymer electrolytes, J. Membr. Sci. 275 (2006) 127–133, https://doi.org/10.1016/j.memsci.2005.09.012.

[15] Z.J. Chang, X.H. Jin, J. Zeng, T.Y. Song, J. Zhang, High photocatalytic activity of covalent grafting of phthalocyanines on crosslinked electrospun PVA/PAA nanofibers, Mater. Sci. Forum 848 (2016) 419–424, https://doi.org/10.4028/www.scientific.net/MSF.848.419.

[16] J. Yun, J.S. Im, Y.S. Lee, H. Il Kim, Electro-responsive transdermal drug delivery behavior of PVA/PAA/MWCNT nanofibers, Eur. Polym. J. 47 (2011) 1893–1902, https://doi.org/10.1016/j.eurpolymj.2011.07.024.

[17] J.C. Park, T. Ito, K.O. Kim, K.W. Kim, B.S. Kim, M.S. Khil, H.Y. Kim, I.S. Kim, Electrospun poly(vinyl alcohol) nanofibers: effects of degree of hydrolysis and enhanced water stability, Polym. J. 42 (2010) 273–276, https://doi.org/10.1038/pj.2009.340.

[18] J.A. Park, S.C. Lee, S.B. Kim, Synthesis of dual-functionalized poly(vinyl alcohol)/poly(acrylic acid) electrospun nanofibers with enzyme and copper ion for enhancing anti-biofouling activities, J. Mater. Sci. 54 (2019) 9969–9982, https://doi.org/10.1007/s10853-019-03578-6.

[19] H. Lee, R. Mensire, R.E. Cohen, M.F. Rubner, Strategies for hydrogen bonding based layer-by-layer assembly of poly (vinyl alcohol) with weak polyacids, Macromolecules 45 (2012) 347–355, https://doi.org/10.1021/ma202092w.

[20] T. Liu, C. Jiao, X. Peng, Y.-N. Chen, Y. Chen, C. He, R. Liub, H. Wang, Super-strong and tough poly(vinyl alcohol)/poly(acrylic acid) hydrogels reinforced by hydrogen bonding, J. Mater. Chem. B. 6 (2018) 8105–8114, https://doi.org/10.1039/C8TB02556H.

[21] M.J.D. Nugent, C.L. Higginbotham, Preparation of a novel freeze thawed poly (vinyl alcohol) composite hydrogel for drug delivery applications, Eur. J. Pharm. Biopharm. 67 (2007) 377–386.

[22] G.G. de Lima, F. Traon, E. Moal, M. Canillas, M.A. Rodriguez, H.O. McCarthy, N. Dunne, D.M. Devine, M.J.D. Nugent, Composite cryogels for dual drug delivery and enhanced mechanical properties, Polym. Compos. 39 (2018) E210–E220, https://doi.org/10.1002/pc.24450.

[23] Y. Zhou, Q. Zhao, M. Wang, Dual release of VEGF and PDGF from emulsion electrospun bilayer scaffolds consisting of orthogonally aligned nanofibers for gastrointestinal tract regeneration, MRS Commun. 9 (2019) 1098–1104, https://doi.org/10.1557/mrc.2019.104.

[24] F. Amini, D. Semnani, S. Karbasi, S.N. Banitaba, A novel bilayer drug-loaded wound dressing of PVDF and PHB/Chitosan nanofibers applicable for post-surgical ulcers, Int. J. Polym. Mater. Polym. Biomater. 68 (2019) 772–777, https://doi.org/10.1080/00914037.2018.1506982.

[25] W. Li, X. Tan, T. Luo, Y. Shi, Y. Yang, L. Liu, Preparation and characterization of electrospun PLA/PU bilayer nanofibrous membranes for controlled drug release applications, Integr. Ferroelectr. 179 (2017) 104–119, https://doi.org/10.1080/10584587.2017.1331113.

[26] H.E. Colley, Z. Said, M.E. Santocildes-Romero, S.R. Baker, K. D'Apice, J. Hansen, L.S. Madsen, M.H. Thornhill, P.V. Hatton, C. Murdoch, Pre-clinical evaluation of novel mucoadhesive bilayer patches for local delivery of clobetasol-17-propionate to the oral mucosa, Biomaterials 178 (2018) 134–146, https://doi.org/10.1016/j.biomaterials.2018.06.009.

[27] D.H. Kim, J. Huegel, B.L. Taylor, C.A. Nuss, S.N. Weiss, L.J. Soslowsky, R.L. Mauck, A.F. Kuntz, Biocompatibility and bioactivity of an FGF-loaded microsphere-based bilayer delivery system, Acta Biomater. 111 (2020) 341–348, https://doi.org/10.1016/j.actbio.2020.04.048.

[28] N. Lavielle, A. Hébraud, L. Thöny-Meyer, R.M. Rossi, G. Schlatter, 3D composite assemblies of microparticles and nanofibers for tailored wettability and controlled drug delivery, Macromol. Mater. Eng. 302 (2017) 1–8, https://doi.org/10.1002/mame.201600458.

[29] K. Chen, G. Chen, S. Wei, X. Yang, D. Zhang, L. Xu, Preparation and property of high strength and low friction PVA-HA/PAA composite hydrogel using annealing treatment, Mater. Sci. Eng. C 91 (2018) 579–588, https://doi.org/10.1016/j.msec.2018.05.080.
[30] K. Kumeta, I. Nagashima, S. Matsui, K. Mizoguchi, Crosslinking reaction of poly(vinyl alcohol) with poly(acrylic acid) (PAA) by heat treatment: effect of neutralization of PAA, J. Appl. Polym. Sci. 90 (2003) 2420–2427, https://doi.org/10.1002/app.12910.
[31] B. Cerroni, E. Chiessi, S. Margheritelli, L. Oddo, G. Paradossi, Polymer shelled microparticles for a targeted doxorubicin delivery in cancer therapy, Biomacromolecules 12 (2011) 593–601, https://doi.org/10.1021/bm101207k.
[32] S. Ghosh, R.S.K. Raju, N. Ghosh, K. Chaudhury, S. Ghosh, I. Banerjee, N. Pramanik, Development and physicochemical characterization of doxorubicin-encapsulated hydroxyapatite–polyvinyl alcohol nanocomposite for repair of osteosarcoma-affected bone tissues, Comptes Rendus Chim. 22 (2019) 46–57, https://doi.org/10.1016/j.crci.2018.10.005.
[33] N. Amani, M. Shokrzadeh, F. Shaki, Clarithromycin effectively enhances doxorubicin-induced cytotoxicity and apoptosis in MCF7 cells through dysregulation of autophagy, Adv. Med. Sci. 65 (2020) 235–243, https://doi.org/10.1016/j.advms.2020.03.002.
[34] N.A. Peppas, E.W. Merrill, Differential scanning calorimetry of crystallized PVA hydrogels, J. Appl. Polym. Sci. 20 (1976) 1457–1465, https://doi.org/10.1002/app.1976.070200604.
[35] H. Ji-Qing, L. Qi, X. Shu-ping, S. Yu-xian, S. Gen-yun, Effect of lumiracoxib on proliferation and apoptosis of human nonsmall cell lung cancer cells in vitro, Chin. Med. J. (Engl.) 121 (2008) 602–607.
[36] Y. Zhao, J. Gao, J. Ji, M. Gao, Q. Yin, Q. Qiu, C. Wang, S. Chen, J. Xu, R. Liang, Y. Cai, X. Wang, Cytotoxicity enhancement in MDA-MB-231 cells by the combination treatment of tetrahydropalmatine and berberine derived from Corydalis yanhusuo W. T. Wang, J. Intercult. Ethnopharmacol. 3 (2014) 68, https://doi.org/10.5455/jice.20140123040224.
[37] T.A.W. Wijanarko, A. Kusumaatmaja, Roto Chotimah, K. Triyana, Effect of heat treatment on morphology and crystallinity of electrospun Poly(vinyl alcohol) nanofibers, AIP Conf. Proc. 1755 (2016), https://doi.org/10.1063/1.4958583.
[38] J. Zeng, H. Hou, J.H. Wendorff, A. Greiner, Electrospun poly(vinyl alcohol)/poly(acrylic acid) fibres with excellent water-stability, E-Polymers 78 (2004), https://doi.org/10.1515/epoly.2004.4.1.899.
[39] B. Felice, M.P. Prabhakaran, M. Zamani, A.P. Rodríguez, S. Ramakrishna, Electrosprayed poly(vinyl alcohol) particles: preparation and evaluation of their drug release profile, Polym. Int. 64 (2015) 1722–1732, https://doi.org/10.1002/pi.4972.
[40] H. Fong, I. Chun, D.H. Reneker, Beaded nanofibers formed during electrospinning, Polymer (Guildf) 40 (1999) 4585–4592, https://doi.org/10.1016/S0032-3861(99)00068-3.
[41] C. Zhang, X. Yuan, L. Wu, Y. Han, J. Sheng, Study on morphology of electrospun poly(vinyl alcohol) mats, Eur. Polym. J. 41 (2005) 423–432, https://doi.org/10.1016/j.eurpolymj.2004.10.027.
[42] S. Kumari, L.K. Pradhan, L. Kumar, M.K. Manglam, M. Kar, Effect of annealing temperature on morphology and magnetic properties of cobalt ferrite nanofibers, Mater. Res. Express 6 (2019).
[43] W. Pan, Z. Ma, J. Liu, Q. Liu, J. Wang, Effect of heating rate on morphology and structure of CoFe 2O4 nanofibers, Mater. Lett. 65 (2011) 3269–3271, https://doi.org/10.1016/j.matlet.2011.06.102.
[44] Z. Wang, N. Cai, Q. Dai, C. Li, D. Hou, X. Luo, Y. Xue, F. Yu, Effect of thermal annealing on mechanical properties of polyelectrolyte complex nanofiber membranes, Fibers Polym. 15 (2014) 1406–1413, https://doi.org/10.1007/s12221-014-1406-2.
[45] G.G. de Lima, R.O. de Souza, A.D. Bozzi, M.A. Poplawska, D.M. Devine, M.J.D. Nugent, Extraction method plays critical role in antibacterial activity of propolis-loaded hydrogels, J. Pharm. Sci. 105 (2016) 1248–1257, https://doi.org/10.1016/j.xphs.2015.12.027.
[46] I.M. Jipa, A. Stoica, M. Stroescu, L.M. Dobre, T. Dobre, S. Jinga, C. Tardei, Potassium sorbate release from poly(vinyl alcohol)-bacterial cellulose films, Chem. Pap. 66 (2012) 138–143, https://doi.org/10.2478/s11696-011-0068-4.
[47] W. Kam, C.W. Liew, J.Y. Lim, S. Ramesh, Electrical, structural, and thermal studies of antimony trioxide-doped poly(acrylic acid)-based composite polymer electrolytes, Ionics (Kiel) 20 (2014) 665–674, https://doi.org/10.1007/s11581-013-1012-0.
[48] A. Aytimur, I. Uslu, Promising materials for wound dressing: PVA/PAA/PVP electrospun nanofibers, Polym. Plast. Technol. Eng. 53 (2014) 655–660, https://doi.org/10.1080/03602559.2013.874031.
[49] J.S. Gaffney, N.A. Marley, D.E. Jones, Fourier Transform Infrared (FTIR) spectroscopy, Charact. Mater. (2012), https://doi.org/10.1016/c2009-0-22072-1.
[50] D.H. Williams, I. Fleming, Infrared spectra, in: Spectrosc. Methods Org. Chem., sixth ed., McGraw-Hill Higher Education, London, 2008.
[51] W. Samprasit, P. Akkaramongkolporn, T. Ngawhirunpat, T. Rojanarata, R. Kaomongkolgit, P. Opanasopit, Fast releasing oral electrospun PVP/CD nanofiber mats of taste-masked meloxicam, Int. J. Pharm. 487 (2015) 213–222, https://doi.org/10.1016/j.ijpharm.2015.04.044.
[52] N.D. Gavrilova, I.A. Malyshkina, E.E. Makhaeva, V.K. Novik, A.V. Vorobiev, Dielectric relaxation anomalies in polyacrylic acid and their relationship with “critical” points of water, Ferroelectrics 504 (2016) 3–14, https://doi.org/10.1080/00150193.2016.1238284.
[53] S. Mollá, V. Compañ, Polyvinyl alcohol nanofiber reinforced Nafion membranes for fuel cell applications, J. Membr. Sci. 372 (2011) 191–200, https://doi.org/10.1016/j.memsci.2011.02.001.
[54] X. Zhu, X. Du, X. Chen, J. Hu, X. Zhou, L. Guo, Determining the effects of annealing time on the glass transition temperature of Pueraria lobata (Willd.) Ohwi starch, Int. J. Food Sci. Technol. 53 (2018) 43–49, https://doi.org/10.1111/ijfs.13518.
[55] Y. Park, S. Lee, S.S. Ha, B. Alunda, D.Y. Noh, Y.J. Lee, S. Kim, J.H. Seol, Crosslinking effect on thermal conductivity of electrospun poly(acrylic acid) nanofibers, Polymers (Basel) 11 (2019) 1–13, https://doi.org/10.3390/polym11050858.
[56] M.J.D. Nugent, C.L. Higginbotham, Investigation of the influence of freeze-thaw processing on the properties of polyvinyl alcohol/polyacrylic acid complexes, J. Mater. Sci. 41 (2006) 2393–2404, https://doi.org/10.1007/s10853-006-7075-9.
[57] J.-S. Park, J.-W. Park, E. Ruckenstein, Thermal and dynamic mechanical analysis of PVA/MC blend hydrogels, Polymer (Guildf) 42 (2001) 4271–4280, https://doi.org/10.1016/S0032-3861(00)00768-0.
[58] D. De la Garza, F. De Santiago, L. Materon, M. Chipara, M. Alcoutlabi, Fabrication and characterization of centrifugally spun poly(acrylic acid) nanofibers, J. Appl. Polym. Sci. 136 (2019) 1–9, https://doi.org/10.1002/app.47480.
[59] M. Lim, D. Kim, J. Seo, Enhanced oxygen-barrier and water-resistance properties of poly(vinyl alcohol) blended with poly(acrylic acid) for packaging applications, Polym. Int. 65 (2016) 400–406, https://doi.org/10.1002/pi.5068.
[60] E. Rynkowska, K. Fatyeyeva, S. Marais, J. Kujawa, W. Kujawski, Chemically and thermally crosslinked PVA-based membranes: effect on swelling and transport behavior, Polymers (Basel) 11 (2019) 1799.